Electronic Supplementary Material (ESI) for Physical Chemistry Chemical Physics.

Supporting Information

Conformational Preferences of Monohydrated Clusters of the Imidazole Derivatives Revisited

Aditi Bhattacherjee[#] and Sanjay Wategaonkar*

Department of Chemical Sciences, Tata Institute of Fundamental Research, Homi Bhabha Road, Mumbai 400 005, India

 # Present address: Chemical Sciences Division, Lawrence Berkeley National Laboratory, 1 Cyclotron Road, Berkeley, California 94720, United States

FIGURES

Figure S1: The normal mode eigenvectors of (a) imidazole and (b) benzimidazole calculated at the MP2/aug-cc-pVDZ level of theory. While the N-H stretching mode is a local oscillator in both molecules, all the C-H stretching modes are coupled in imidazole. Fusing it with a six-membered ring in benzimidazole renders the C(2)-H a local oscillator.

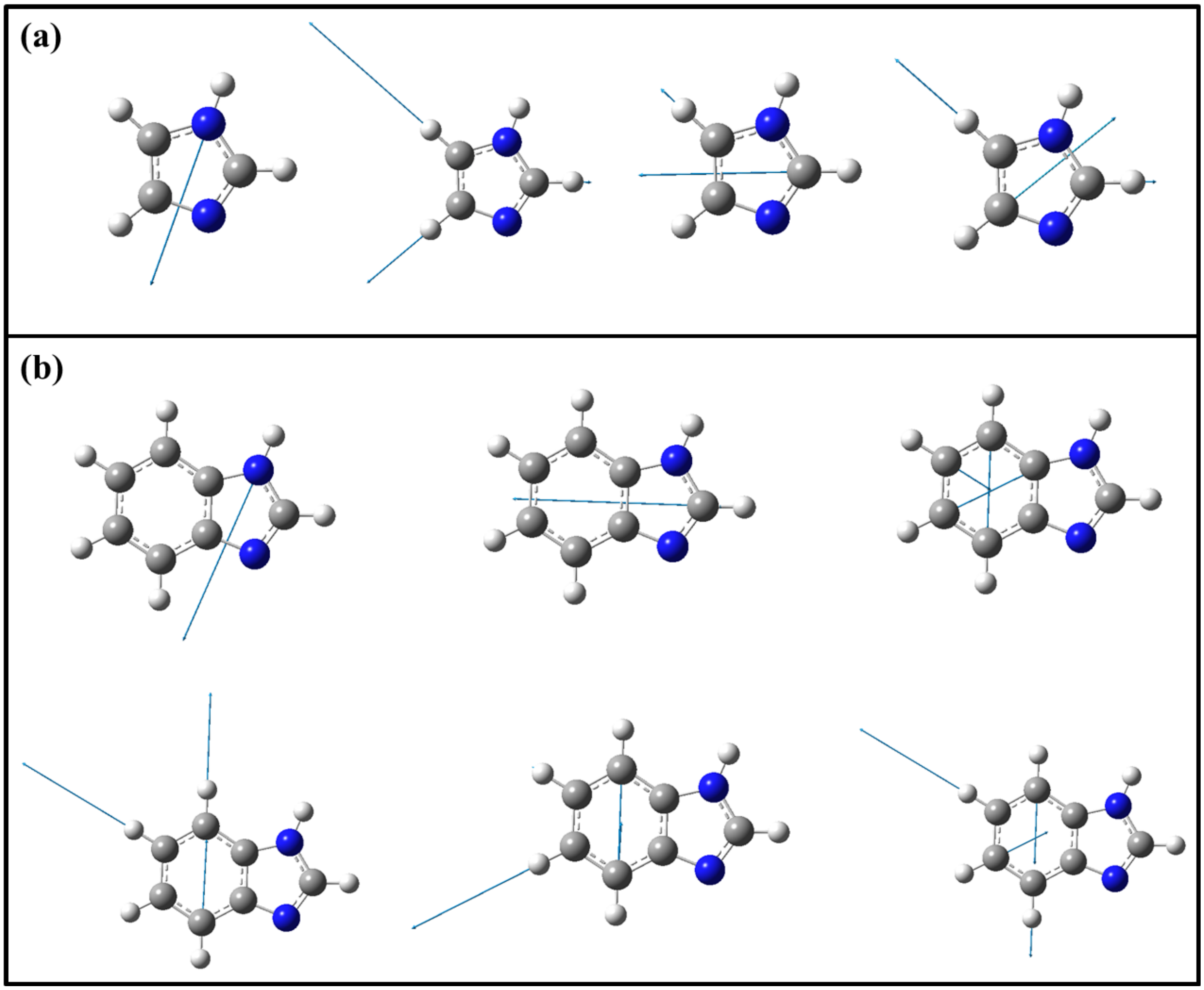

Figure S2: Action spectra of clusters of BIM with water (scaled up in intensity by a factor of 4 to make the weak features due to photo-fragmentation prominent) obtained by monitoring the monomer mass channel. The time delay between the pulsed valve opening and the laser pulse was optimized for the higher water cluster masses instead of the monomer mass (in contrast to the spectrum shown in Figure 2d which was optimized for BIM monomer). The strong feature at 36022 cm^{-1} is the band origin of the monomer. Traces (a) to (d) correspond to decreasing water concentration in the buffer gas line which shifts the equilibrium from higher to lower water clusters of the solute. Features enclosed by brackets arise due to fragmentation. The starred peak is a hot band of the monomer.

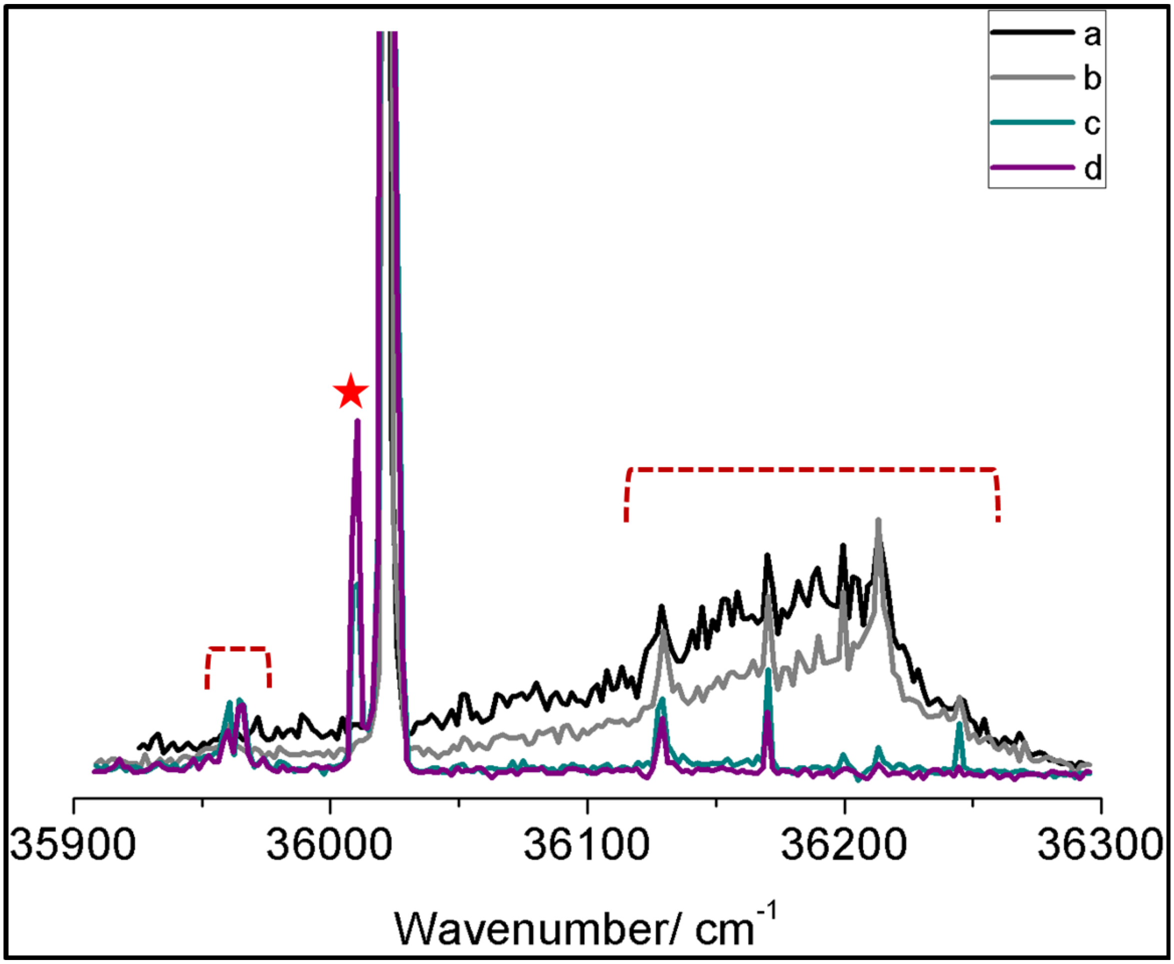

Figure S3: FDIR spectra of the BIM-W_1 complexes corresponding to the features in the electronic spectra [A' (trace a), A (trace c), and B (trace d), as indicated on the right]. The computed stick spectra at the MP2/aug-cc-pVDZ level (without counterpoise (cp) correction) scaled by 0.9620 are shown for comparison. The spectral predictions are qualitatively similar to those shown in Figure 6 of the main article. Comparison of the computed frequencies with and without cp correction is summarized in Table S3.

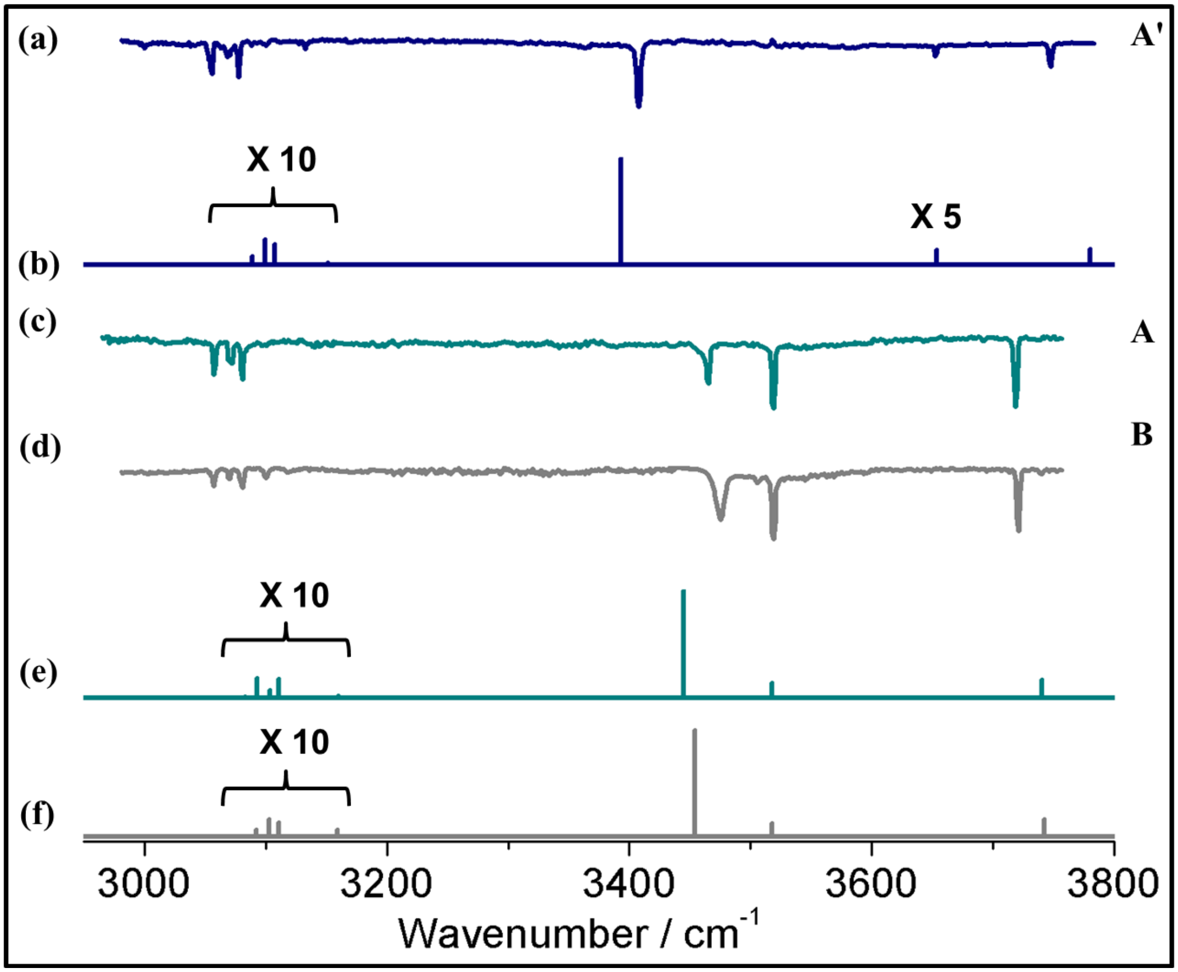

Figure S4: FDIR spectra of the MBIM-W$_1$ complexes corresponding to the features in the electronic spectra [A (trace a), and B (trace b), as indicated on the right]. The computed stick spectra at the MP2/aug-cc-pVDZ level (without counterpoise (cp) correction) scaled by 0.9620 are shown for comparison. The spectral predictions are qualitatively similar to those shown in Figure 7 of the main article. Comparison of the computed frequencies with and without cp correction is summarized in Table S3.

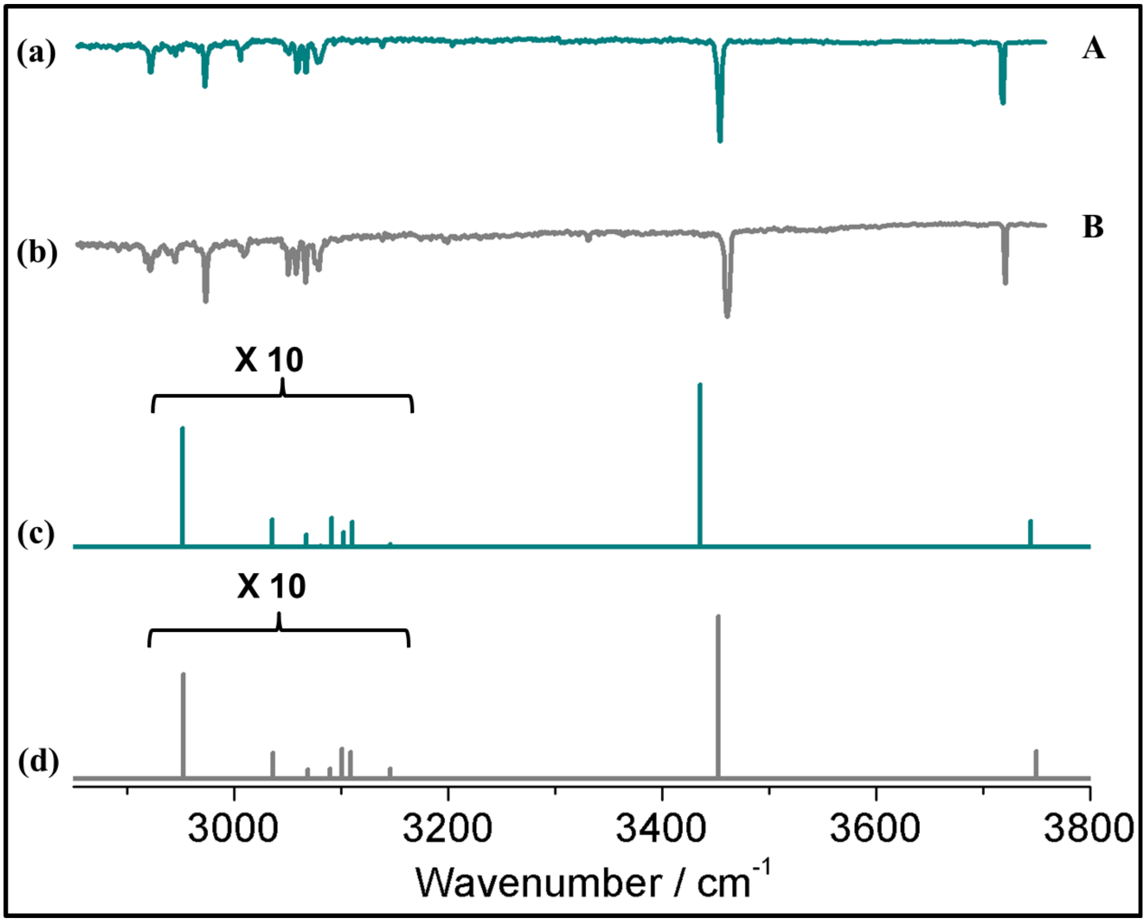

Figure S5: Molecular graphs obtained for the optimized structures of BIM-W_1 and MBIM-W_1 at the MP2/ aug-cc-pVDZ level of theory.

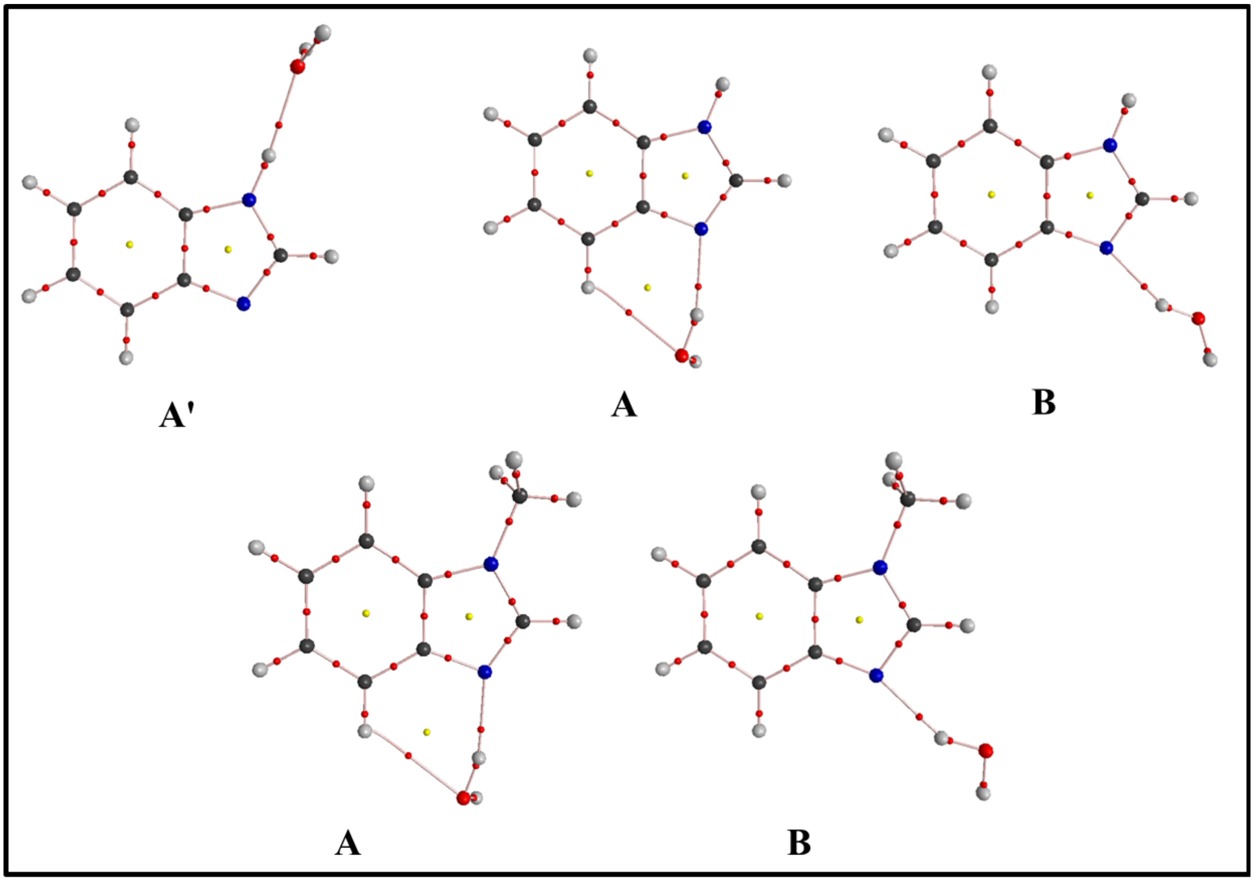

Figure S6: Equilibrium structures of (a) C(2)-H···O bound and (b) O-H···π bound conformers of MBIM-W$_1$ complex obtained at cp-MP2/ aug-cc-pVDZ level. Monohydrates of BIM did not give stable structures that were C(2)-H···O or O-H···π bound at this level of theory.

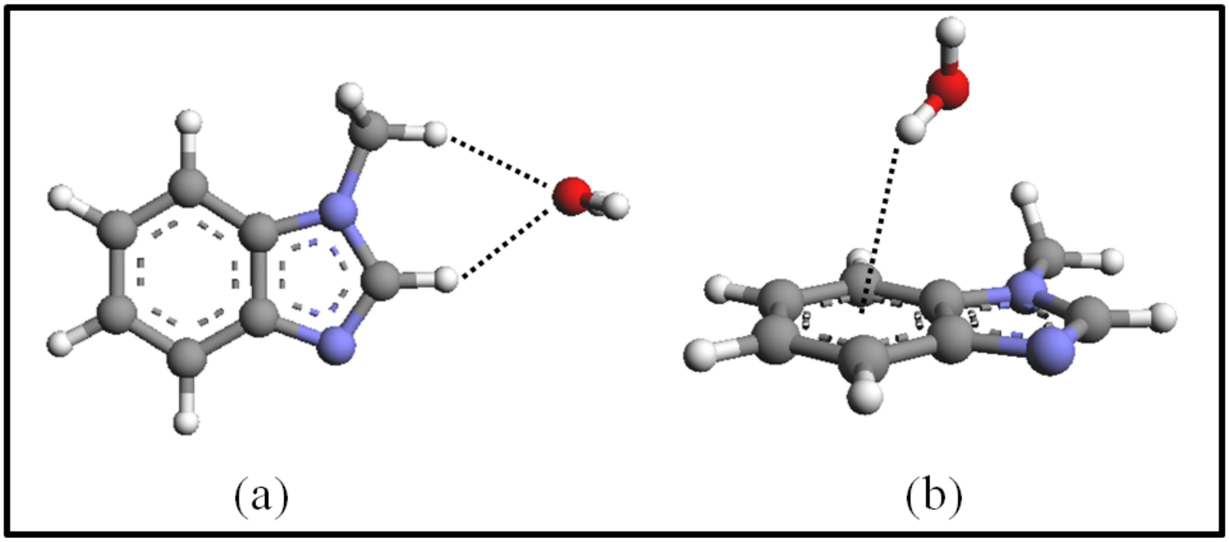

Figure S7: Equilibrium structure of BIM-W$_1$ with a linear O-H···N hydrogen bond (∠ O-H-N = 176.2°) obtained at the B3LYP/ aug-cc-pVDZ level.

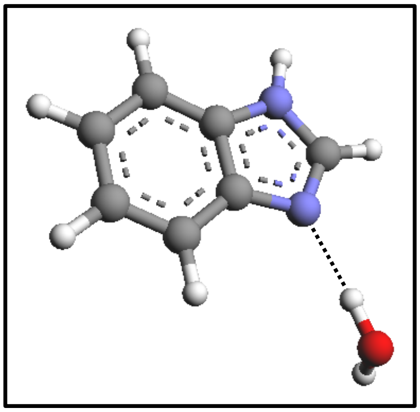

Figure S8: Equilibrium structures of O-H···N and N-H···O conformers of 1:1 water clusters of imidazole (IM), 4-methylimidazole (4MIM), 5-methylimidazole (5MIM), 4-phenylimidazole (4PHIM), 5-phenylimidazole (5PHIM), and histidine (HIS) obtained at the cp-MP2/ aug-cc-pVDZ level. The binding energy values (kcal mol^{-1}) are provided in parentheses.

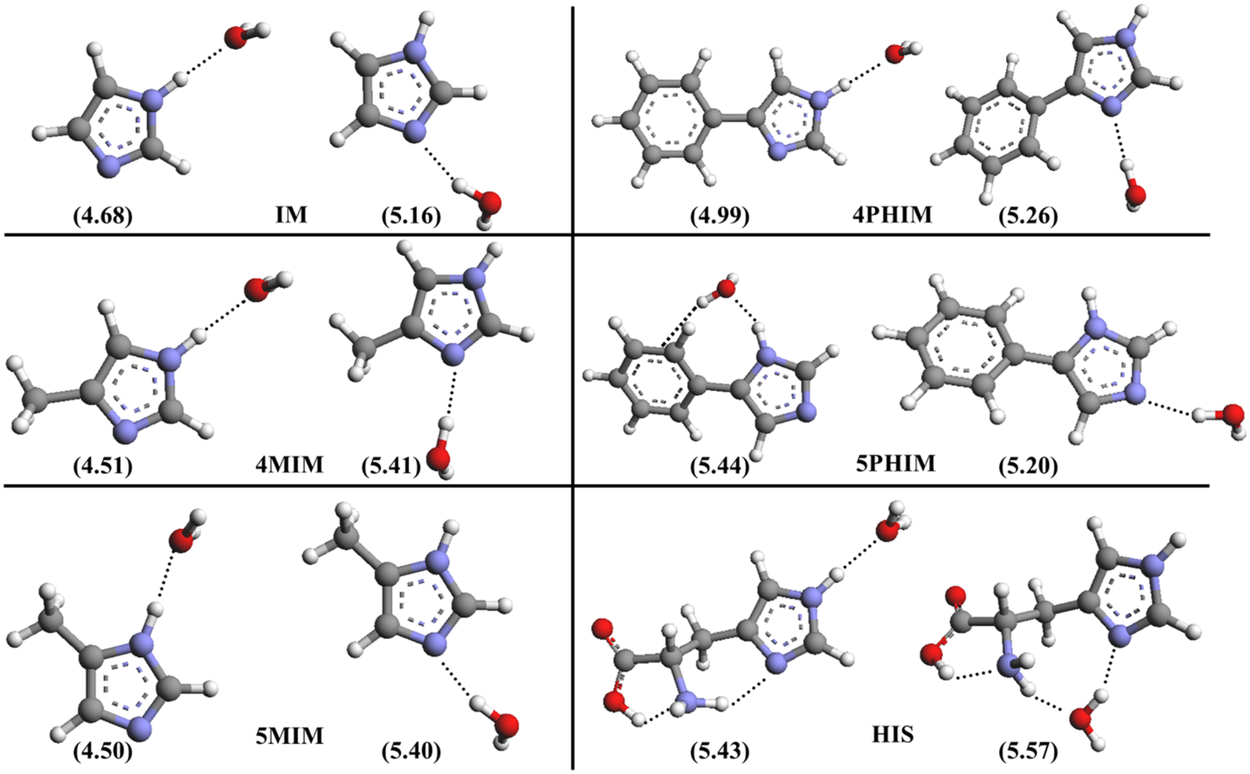

TABLES

Tables S1 and S2 list all the data used for the assignment of the C(2)-H stretching mode in BIM and MBIM, respectively, with the help of quantum chemical calculations. The top row in each table gives the experimentally observed stretching frequencies. Two possibilities exist for the assignment of the C(2)-H stretching mode: 3134 cm^{-1}/ 3095 cm^{-1} (in BIM) and 3132 cm^{-1}/ 3103 cm^{-1} (in MBIM). The subsequent rows indicate the scaled computed frequencies for the stretching modes obtained at various levels of calculation. I and II indicate the basis sets 6-311++G** and aug-cc-pVDZ, respectively. The scaling factor (enclosed in parentheses) was obtained by matching the computed NH stretching mode in BIM with the observed value (3519 cm^{-1}). The computed frequencies of the fundamental C-H stretches of both BIM and MBIM were also uniformly scaled by the same factor indicated for each level of calculation. Since the phenyl ring CH modes are known with certainty from our experiments, the mean deviation of these modes from the observed ones were determined [Mean Δ(C-H)]. The scaled calculated C(2)-H frequency was then corrected by the mean value of Δ(C-H). The observed stretch at 3095 cm^{-1} agrees better with the corrected C(2)-H value and is therefore assigned as the C(2)-H in BIM. Similarly, the observed stretch at 3103 cm^{-1} agrees better with the corrected C(2)-H value and is therefore assigned as the C(2)-H in MBIM.

Table S1: Data for the C(2)-H stretching mode assignment in BIM with the help of quantum chemical calculations. I and II denote the basis sets 6-311++G** and aug-cc-pVDZ, respectively.

Modes	N-H	C(2)-H	(C-H)$_1$	(C-H)$_2$	(C-H)$_3$		
Observed	3519	(3134/3095)	3080	3068	3055		
Scaled computed frequencies						Mean Δ(C-H)	Corrected C(2)-H
Level/ basis set (Scaling factor)	N-H	C(2)-H	(C-H)$_1$	(C-H)$_2$	(C-H)$_3$		
B3LYP/ I (0.9619)	3519	3109	3075	3066	3055	2.29	3111
B3LYP/ II (0.9634)	3519	3124	3087	3078	3067	-9.72	3114
M06-2X / I (0.95)	3519	3078	3053	3047	3036	22.65	3100
M06-2X/ II (0.9534)	3519	3093	3063	3056	3045	12.81	3106
ωB97X-D/ I (0.9483)	3519	3089	3061	3052	3042	15.63	3104
ωB97-xD/ II (0.9494)	3519	3105	3075	3067	3055	2.07	3107
LC-ωPBE/ I (0.9433)	3519	3086	3067	3059	3048	9.60	3096
LC-ωPBE/ II (0.9445)	3519	3103	3081	3072	3061	-3.61	3099
MP2/ I (0.9571)	3519	3132	3094	3086	3076	-17.46	3114
MP2/ II (0.9620)	3519	3155	3110	3101	3090	-32.87	3122

Table S2: Data for the C(2)-H stretching mode assignment in MBIM with the help of quantum chemical calculations. I and II denote the basis sets 6-311++G** and aug-cc-pVDZ, respectively.

Modes	C(2)-H	(C-H)$_1$	(C-H)$_2$	(C-H)$_3$		
Observed	3132/3103	3077	3065	3056		
Computed frequencies					Mean Δ(C-H)	Corrected C(2)-H
Level/ basis set (Scaling factor)	C(2)-H	(C-H)$_1$	(C-H)$_2$	(C-H)$_3$		
B3LYP/ I (0.9619)	3098	3074	3066	3055	1.00	3099
B3LYP/ II (0.9634)	3115	3087	3079	3068	-11.78	3103
M06-2X / I (0.95)	3067	3055	3046	3035	20.50	3088
M06-2X/ II (0.9534)	3086	3070	3059	3048	7.16	3094
ωB97X-D/ I (0.9483)	3077	3060	3051	3040	15.72	3092
ωB97-xD/ II (0.9494)	3092	3072	3064	3052	3.36	3096
LC-ωPBE/ I (0.9433)	3076	3066	3058	3047	8.92	3085
LC-ωPBE/ II (0.9445)	3093	3080	3071	3061	-4.47	3088
MP2/ I (0.9571)	3118	3092	3084	3073	-16.85	3101
MP2/ II (0.9620)	3141	3108	3100	3088	-32.76	3108

Table S3: Comparison of the experimentally observed fundamental stretching modes in the conformers of BIM-W$_1$ and MBIM-W$_1$ with those calculated at MP2/ aug-cc-pVDZ with and without counterpoise correction. Calculated frequencies have been scaled by a uniform scaling factor of 0.9620. The assignment of the modes is provided in the last column. Bold numbers in parentheses in columns 3 and 4 indicate the deviation of the computed frequency from the experimental number for the important H-bond donor stretching modes. It can be seen that the agreement is within 7 cm^{-1} when counterpoise correction is employed and slightly higher (~10-20 cm^{-1}) in the absence of it. The computed free OH/ NH stretches are reasonably close at the two levels (within 5 cm^{-1}) whereas the ring CH modes are near identical (within 1 cm^{-1}).

BIM-W$_1$	Observed	cp-MP2/ aug-cc-pVDZ	MP2/ aug-cc-pVDZ	Assignment
A'	3748	3782	3780	O-H, antisymmetric
	3652	3656	3654	O-H, symmetric
	3408	3410 **(2)**	3393 **(-15)**	Bound NH
	3100	3152	3151	C(2)-H
	3078, 3068, 3056, —	3107, 3099, 3088, 3078(w)	3107, 3099, 3089, 3079(w)	C-H, phenyl
A	3719	3744	3741	O-H, free
	3519	3518	3518	N-H, free
	3465	3471 **(6)**	3444 **(-21)**	O-H, bound
	3097	3159	3159	C(2)-H
	3081, 3072, 3057, —	3110, 3103, 3092, 3083(w)	3111, 3104, 3093, 3083(w)	C-H, phenyl
B	3721	3746	3742	O-H, free
	3519	3518	3518	N-H, free
	3475	3479 **(4)**	3454 **(-21)**	O-H, bound
	3100	3158	3159	C(2)-H
	3081, 3069, 3057, —	3111, 3102, 3092, 3083(w)	3111, 3103, 3092, 3083(w)	C-H, phenyl

MBIM-W$_1$	Observed	cp-MP2/ aug-cc-pVDZ	MP2/ aug-cc-pVDZ	Assignment
A	3719	3744	3744	O-H, free
	3454	3461 **(7)**	3436 **(-18)**	O-H, bound
	—	3145	3146	C(2)-H
	3078, 3067, 3059	3109, 3101, 3090, 3081(w)	3111, 3102, 3091, 3081(w)	C-H, phenyl
	3051, 3006, 2973, —	3068, 3036, 2952	3067, 3036, 2952	C-H, methyl
B	3721	3745	3750	O-H, free
	3461	3468 **(7)**	3452 **(-9)**	O-H, bound
	—	3146	3146	C(2)-H
	3078, 3067, 3058	3109, 3101, 3090, 3081(w)	3109, 3101, 3090, 3081(w)	C-H, phenyl
	3051, 3009, 2974, —	3069, 3036, 2952	3069, 3036, 2952	C-H, methyl

Table S4: Hydrogen bonding parameters, the ZPE corrected binding energies, and the OH stretching frequencies for the equilibrium structures of (a) C(2)-H···O bound MBIM-W$_1$ and (b) O-H···π bound MBIM-W$_1$ shown in Figure S6 at the cp-MP2/aug-cc-pVDZ level. The frequencies were scaled by 0.9620.

Parameters	(a)	(b)
r(H···Y) (Å)	2.543 / 2.543	2.933
R(X···Y) (Å)	3.514 / 3.586	3.811
Δ X-H (mÅ)	-0.25/ -0.21	3.68
∠X-H-Y (°)	147.9 / 158.3	151.1
D_0 (kcal mol^{-1})	2.37	3.64
ν_{O-H}, free (cm^{-1}) ν_{O-H}, bound (cm^{-1})	3777 3651	3757 3619

Table S5: Hydrogen bonding parameters, the ZPE and BSSE corrected binding energies, and OH/NH stretching frequencies for the optimized structure of BIM-W$_1$ shown in Figure S7 at the B3LYP/6-311++G** and B3LYP/aug-cc-pVDZ levels. The frequencies were scaled by 0.9619 and 0.9634, respectively.

Parameters	B3LYP/6-311++G**	B3LYP/aug-cc-pVDZ
r(H···Y) (Å)	1.947	1.928
R(X···Y) (Å)	2.924	2.906
Δ X-H (mÅ)	14.59	14.56
∠X-H-Y (°)	178.1	176.2
D_0 (kcal mol^{-1})	4.89	4.46
ν_{O-H}, free (cm^{-1}) ν_{N-H}, free (cm^{-1}) ν_{O-H}, bound (cm^{-1})	3735 3519 3437	3726 3519 3402